

ARTICLE



Acetylation licenses Th1 cell polarization to constrain *Listeria monocytogenes* infection

Yanan Sophia Zhang^{1,2,10}, Dazhuan Eric Xin^{3,10}, Zhizhang Wang^{4,10}, Wenlong Peng², Yuanyuan Zeng⁵, Jianshu Liang², Mengmeng Xu^{2,6}, Nannan Chen², Jie Zhang², Jicheng Yue², Mengtao Cao⁷, Chenxi Zhang³, Yuting Wang², Zhijie Chang⁸, Xiao-mei Lu⁹, Lei Chang² and Y. Eugene Chinn^{1,2}✉

© The Author(s), under exclusive licence to ADMC Associazione Differenziamento e Morte Cellulare 2022

T helper 1 (Th1) immunity is typically viewed as a critical adaptation by vertebrates against intracellular pathogens. Identifying novel targets to enhance Th1 cell differentiation and function is increasingly important for anti-infection immunity. Here, through small-molecule screening focusing on epigenetic modifiers during the *in vitro* Th1 cell differentiation process, we identified that the selective histone deacetylase 6 (HDAC6) inhibitors ricolinostat and nexturastat A (Nex A) promoted Th1 cell differentiation. HDAC6-depleted mice exhibit elevation of Th1 cell differentiation, and decreased severity of *Listeria monocytogenes* infection. Mechanistically, HDAC6 directly deacetylated CBP-catalyzed acetylation of signal transducer and activator of transcription 4 (STAT4)-lysine (K) 667 via its enzymatic activity. Acetylation of STAT4-K667 is required for JAK2-mediated phosphorylation and activation of STAT4. *Stat4*^{K667R} mutant mice lost the ability to normally differentiate into Th1 cells and developed severe *Listeria* infection. Our study identifies acetylation of STAT4-K667 as an essential signaling event for Th1 cell differentiation and defense against intracellular pathogen infections, and highlights the therapeutic potential of HDAC6 inhibitors for controlling intracellular pathogen infections.

Cell Death & Differentiation (2022) 29:2303–2315; <https://doi.org/10.1038/s41418-022-01017-9>

INTRODUCTION

IL-12 promotes Th1 cell differentiation and augments IFN γ production through STAT4 activation. In mice, deficiency or inactivation of STAT4 significantly impairs Th1 cell differentiation [1–3]. As research on STATs has progressed over the years, it has become clear that STAT proteins are subject to important posttranslational modifications (PTMs), such as acetylation which heavily affects their dimerization, nuclear translocation and DNA-binding ability [4]. However, STAT4 is the only STAT family member that has not been studied for acetylation.

Histone acetyltransferases (HATs) and HDACs/sirtuins control the acetylation of lysine residues. HDAC6 plays multiple roles in immune pathway and exerts different effects on different T cell subsets [5–8]. In *Hdac6*^{-/-} mice, the percentage of interleukin-17-secreting $\gamma\delta$ T cells increased [9]. Tregs from *Hdac6*^{-/-} mice exhibit enhanced immunosuppressive activity, and administration of HDAC6 inhibitors substantially ameliorates colitis progression in mice [10]. To date, whether HDAC6 is involved in Th1 cell differentiation and bacterial disease remains elusive. Two studies

reported that the ricolinostat significantly augments the percentage and the antitumor characteristics of IFN γ ⁺ CD4⁺ T cells in myeloma [11, 12]. Although both pan- and selective-HDACis have the potential to modulate the functions of all types of cells, their effects on T cells and on IFN γ -secreting Th1 cells in particular are not fully illustrated.

Listeria monocytogenes is an intracellular pathogen of humans and animals and is widely used as a model organism in studying bacterial pathogenesis and host defense [13]. A previous study showed that IL-12 does not play a direct role in the early innate immune clearance of *L. monocytogenes*, but IL-12-dependent IFN γ production is important for generating Th1 cells and shaping the ensuing inflammatory response [3, 14]. Individuals with IFN γ deficiency are more susceptible to environmental pathogens. Therefore, identifying new mechanisms involved in Th1 cell differentiation is crucial for the development of new therapeutic strategies against *Listeria* infection.

Here, we screened a library of chemical compounds targeting epigenetic enzymes for their potential roles in the Th1 cell

¹Institute of Clinical Medicine, Zhejiang Provincial People's Hospital of Hangzhou Medical College, 158 Shangtang Road, Hangzhou, Zhejiang 310000, China. ²Institutes of Biology and Medical Sciences, School of Radiation Medicine and Protection School of Radiological and Interdisciplinary Science, Soochow University, 199 Ren'ai Road, Suzhou, Jiangsu 215123, China. ³Institute of Health Sciences, Shanghai Institutes for Biological Sciences, Chinese Academy of Sciences, 320 Yueyang Road, Shanghai 200031, China. ⁴Department of Pathology, Nanfang Hospital, Southern Medical University, Guangzhou, Guangdong 510515, China. ⁵Department of Respiratory Medicine, the First Affiliated Hospital of Soochow University, Suzhou, Jiangsu 215006, China. ⁶Department of Pathology, the Second Affiliated Hospital of Soochow University, Suzhou, Jiangsu 215000, China. ⁷Department of Respiratory and Critical Care Medicine, Shenzhen Longhua District Central Hospital, Guangdong Medical University Affiliated Longhua District Central Hospital, Shenzhen 518300, China. ⁸State Key Laboratory of Membrane Biology, Tsinghua University School of Medicine, 100084 Beijing, China. ⁹Clinical Medical Research Institute, First Affiliated Hospital of Xinjiang Medical University, Xinjiang Uygur Autonomous Region, Urumqi 830011, China. ¹⁰These authors contributed equally: Yanan Sophia Zhang, Dazhuan Eric Xin, Zhizhang Wang. ✉email: chinyue@suda.edu.cn

Edited by Y. Shi

Received: 9 November 2021 Revised: 7 May 2022 Accepted: 8 May 2022

Published online: 25 May 2022

differentiation process and identified ricolinostat and Nex A obviously promote Th1 cell differentiation and decrease *Listeria* infection in mice. With a series of in vivo and in vitro assays, we proved that HDAC6 directly deacetylates CBP-catalyzed acetylation of STAT4-K667, established HDAC6's function in regulating the Th1 cell differentiation process, and provided selective HDAC6 inhibitors as potential therapies for intracellular bacterial infectious diseases.

RESULTS

Epigenetic compound library screening identifies HDAC6 as an inhibitor of Th1 cell differentiation

To explore the protein modifier landscape of Th1 cell differentiation, mouse primary CD4⁺ T cells were treated with a library of compounds targeting epigenetic enzymes, including HATs, HDACs, methyltransferases, demethylases and so on, while they were primed to the Th1 subtype. We used quantitative polymerase chain reaction (qPCR) indexing of *Irfg* to identify compounds that interfered with the Th1 cell differentiation process (Fig. S1A). We identified a set of compounds that enhanced *Irfg* expression over vehicle treatment by sixteen fold or more (Fig. 1A). Among these lead compounds were four inhibitors that target HDACs: quisinostat, oxamflatin, vorinostat and ricolinostat. The former three are paninhibitors of HDACs; however, the last one, ricolinostat, is a selective inhibitor of HDAC6. We then analyzed all the selective inhibitors of HDAC6 and three of them significantly promoted Th1 cell differentiation (Fig. 1B). The convergent effects of chemically dissimilar compounds suggested that the effects were exerted through HDAC6 inhibition. Through flow cytometry analysis, we confirmed that the HDAC6 inhibitors enhanced Th1 cell differentiation (Fig. 1C, D).

With *Listeria* infection model, we found that Nex A and ricolinostat obviously reduced *Listeria* burdens and increased the survival rate of WT mice over time (Fig. 1E, F and Fig. S1B). Compared with saline treatment, the administration of HDAC6 inhibitors profoundly increased the number of Th1 cells in the spleen and liver of *Listeria*-infected mice (Fig. 1G, H); however, the HDAC6 inhibitors displayed a minor effect on the amount of cytotoxic CD8⁺ IFN γ ⁺ T cells (Fig. S1C, D). These findings provide Nex A and ricolinostat as potential therapeutic drugs for preventing intracellular pathogen infection and suggest that HDAC6 is involved in the Th1 cell differentiation process.

HDAC6-deficient mice are resistant to *Listeria* infection

We further confirmed that HDAC6 deficiency leads to enhanced Th1 cell polarization (Fig. 2A, B and Fig. S2A). *Hdac6* deficiency in mice was confirmed with qPCR (Fig. S2B). Knockdown of HDAC6 in WT CD4⁺ T cells consistently enhanced Th1 cell differentiation (Fig. S2C–E). HDAC6 depletion also increased Th17 cell differentiation but exhibited less of an effect on Treg cell differentiation (Fig. S2F, G). Since Th17 cells mainly mediate adaptive immunity against extracellular bacterial infection, we focused on how HDAC6 regulates Th1 cell-mediated immunity in the following study.

Olga Moreno-Gonzalo et al. reported in 2017 that during the first hours to 24 h of *Listeria* infection, *Hdac6*^{-/-} bone marrow-derived dendritic cells (BMDCs) were less efficient in clearing *Listeria* than WT BMDCs. However, they observed that HDAC6 depletion exhibited a protective effect against *Listeria* infection from 3 to 10 days postinoculation [15], strongly indicating that HDAC6 plays different roles in regulating innate and adaptive immunity. In our experimental setting, we found that bone marrow-derived macrophages (BMDMs) from WT and *Hdac6*^{-/-} mice under IFN γ -treatment expressed comparable amounts of the IFN-stimulated genes *Cxcl9*, *Cxcl10*, *Ccl5*, *Icam* and *iNOS2* and the proinflammatory cytokines *Il6*, *Tnfa* and *Il1 β* (Fig. S2H). However, *Hdac6*^{-/-} mice were more resistant to *Listeria* infection,

had less bacterial load in the spleen and liver on day 5 postinfection and exhibited an increased survival rate compared with WT mice (Fig. 2C, D). Meanwhile, the accumulation of Th1 cells increased obviously in the spleen and liver of *Listeria*-infected *Hdac6*^{-/-} mice compared with WT mice (Fig. 2E, F).

We further isolated naïve CD4⁺ T cells from WT or *Hdac6*^{-/-} mice and adoptively transferred them into *Rag2*^{-/-} mice devoid of T and B cells. After successful reconstitution, *Hdac6*^{-/-} CD4⁺ T cell-reconstituted *Rag2*^{-/-} mice accumulated more Th1 cells than WT CD4⁺ T cell-reconstituted mice (Fig. S2I). None of the reconstituted *Rag2*^{-/-} mice died during the 5 days post *Listeria* infection. However, we found that compared with WT CD4⁺ T cell-transferred mice, adoptive transfer of *Hdac6*^{-/-} CD4⁺ T cells into *Rag2*^{-/-} mice significantly decreased bacterial burden (Fig. 2G). As expected, Th1 cells were more abundant in the spleen and liver of *Hdac6*^{-/-} CD4⁺ T cells reconstituted *Rag2*^{-/-} mice (Fig. 2H, I), suggesting that *Hdac6*^{-/-} CD4⁺ T cells have a higher potential to differentiate into Th1 cells.

These results demonstrate a critical role of HDAC6 in inhibiting the differentiation and antibacterial immunity of Th1 cells; however, the underlying mechanism needs to be investigated further.

HDAC6 and CBP reversibly modify the acetylation pattern of STAT4

With mass spectrometric analysis, HDAC6 was identified as a STAT4-binding protein (Fig. S3A). The interaction between STAT4 and HDAC6 was confirmed through a co-IP assay, both ectopically and endogenously (Fig. 3A, B). In CD4⁺ T cells, IL-12 induced acetylation of STAT4, which was recognized by a pan acetyllysine antibody (Fig. 3C). Meanwhile, STAT4 acetylation intensity was preferentially elevated in differentiated Th1 cells compared with Th0 cells (Fig. 3D). Interestingly, HATs inhibitors from the epigenetic compound library evenly decreased Th1 cell polarization (Fig. 3E, F and Fig. S2B). We further found that CBP is the major acetyltransferase of STAT4 (Fig. 3G). STAT4 and CBP formed complexes in CD4⁺ T cells (Fig. 3H) and in HEK293T cells overexpressed with STAT4 and CBP (Fig. S3C). STAT4 acetylation level was obviously decreased in SGC-CBP30-treated CD4⁺ T cells compared with that in control cells (Fig. S3D). CBP greatly enhanced the transcriptional activity of STAT4 in luciferase assay (Fig. S3E). Knockdown of CBP in CD4⁺ T cells obviously decreased Th1 cell polarization (Fig. 3I and Fig. S3F). The results indicated that CBP enhanced STAT4 transcriptional activity by acetylating its lysine residues.

As expected, CBP-mediated STAT4 acetylation was abolished by HDAC6 both in vivo and in vitro (Fig. 3J, K). We constructed inactive HDAC6 by mutating the critical histidine residue H216 and H611 into alanine (A) separately or simultaneously. HDAC6-H216A did not jeopardize HDAC6 enzymatic activity; however, HDAC6-H611A and HDAC6-H216, 611A completely lost deacetylase activity, indicating that the HDAC6 H611 enzymatic site was responsible for STAT4 deacetylation (Fig. 3J). Therefore, these observations show that HDAC6 and CBP are involved in the Th1 cell differentiation process by reversibly manipulating STAT4 acetylation.

Acetylation of STAT4-K667 is required for Th1 cell differentiation

We constructed vectors expressing STAT4 with K-to-arginine (R) mutations that mimic the loss of acetylation status or a tyrosine (Y)-to-phenylalanine (F) mutation that abrogates tyrosine phosphorylation. Among all the K-to-R mutants tested, only STAT4-K667R lost the transcriptional activity, which was quite similar to STAT4-Y693F (Fig. 4A). K667 and K691 of STAT4 were demonstrated to be acetylated lysine residues via mass spectrometric analysis (Fig. 4B). However, STAT4-K691R exhibited normal transcriptional activity (Fig. 4A). Only STAT4-K667R reduced the

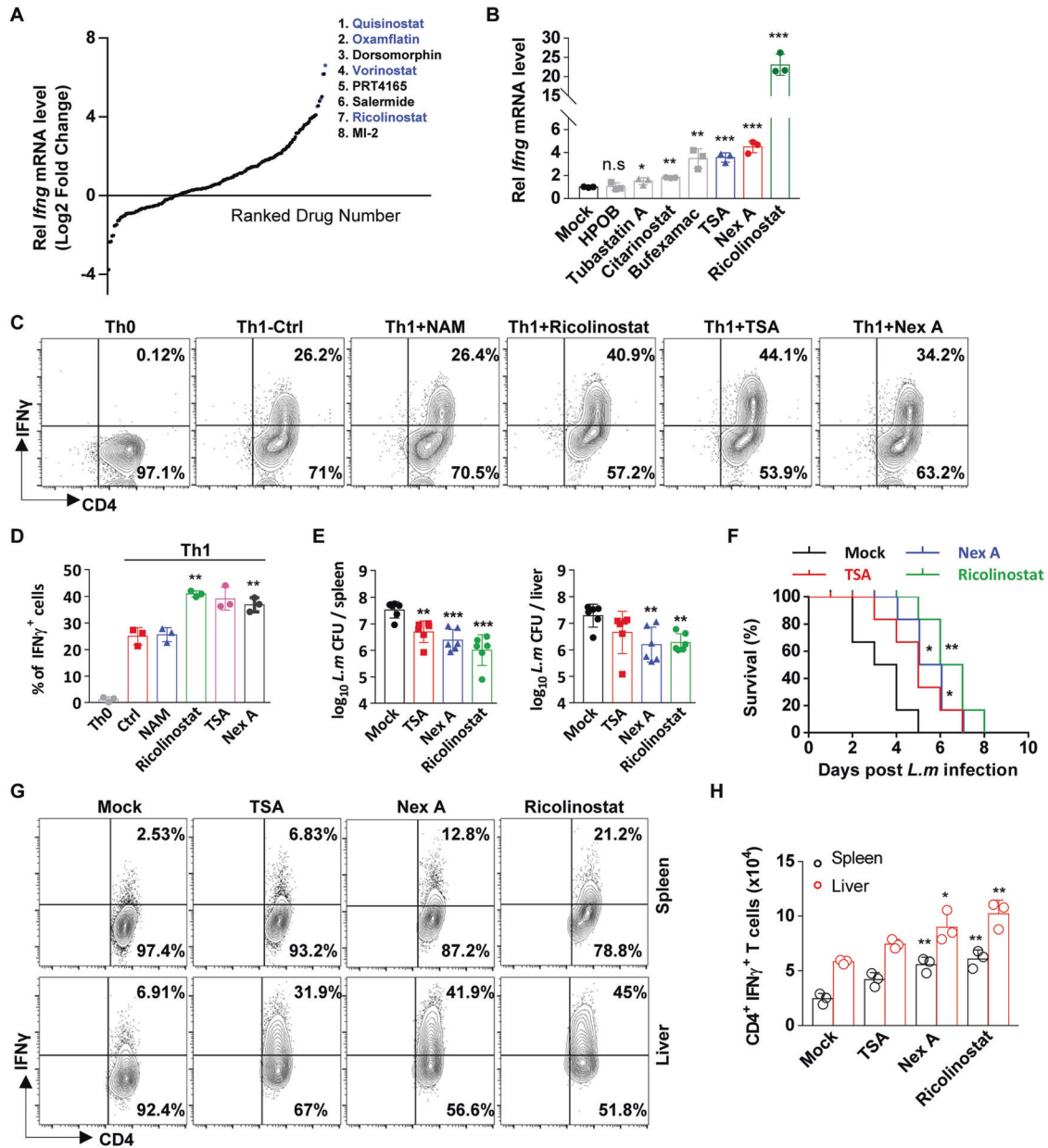


Fig. 1 Epigenetic compound library screening identifies HDAC6 as an inhibitor of Th1 cell differentiation. **A** Relative expression of *Ifng* in CD4⁺ T cells on day 3 of induction into Th1 cell subsets treated with epigenetic compounds (black dots). The top eight compounds that induced expression of *Ifng* by more than sixteen-fold over that induced by vehicle (mock) treatment are listed on the right. Blue dots, compounds that preferentially target HDAC. **B** qPCR analysis of the mRNA level of *Ifng* in CD4⁺ T cells on day 3 of induction into Th1 cell subsets in the absence or presence of HDACs inhibitors. TSA, trichostatin. Representative fluorescence-activated cell sorting (FACS) plots (**C**) and population frequencies (**D**) of Th1 cells polarized in the presence or absence of the indicated inhibitors are shown. **E** *Listeria* CFUs per spleen (left) and liver (right) of WT mice infected with 1×10^4 *L. monocytogenes* i.v. and treated with vehicle saline (mock), TSA (1 mg/kg), Nex A (3 mg/kg) or Ricolinostat (3 mg/kg) accordingly i.p. Mice were sacrificed for the following analysis on day 5 post infection. Colored dots represent individual mice ($n = 6$). Bars represent the mean log CFU/organ. **F** Survival rate of mice from Fig. 1E ($n = 7$). **G**, **H** Representative FACS plots (**G**) and cell number (**H**) of CD4⁺ IFN γ ⁺ T cells in the spleen and liver of mice from Fig. 1E are shown. The data are shown as the mean \pm SD of three independent experiments. * $p < 0.05$, ** $p < 0.01$ and *** $p < 0.001$, n.s means not significant (Student's *t* test).

CBP-catalyzed acetylation intensity, and neither the K691R, K673R mutant nor C-terminal domain-deleted STAT4 affected the acetylation level of STAT4 (Fig. S4A, B). STAT4-K667 is located in its SH2 domain and is highly conserved among STAT family proteins and among different species (Fig. 4C and Fig. S4C). Then, we generated a rabbit polyclonal antibody specifically recognizing acetylation on STAT4-K667 (Fig. S4D). We validated that CBP indeed acetylated STAT4-K667 (Fig. 4D). Moreover, acetylation of STAT4-K667 was observed in Th1 cells (Fig. 4E). SGC-CBP30

significantly decreased STAT4-K667 acetylation (Fig. 4F); however, TSA and Nex A obviously enhanced STAT4-K667 acetylation intensity in Th1 cells (Fig. 4G). Furthermore, HDAC6 directly deacetylated the STAT4-K667 acetyl peptide (Fig. 4H). These findings prove that CBP and HDAC6 reversibly modify the acetylation of STAT4-K667 in Th1 cells.

STAT4 deficiency significantly impaired Th1 cell differentiation (Fig. S4E, F). By reconstituting WT or mutant STAT4 in *Stat4*^{-/-} CD4⁺ T cells, we found that neither STAT4-K667R nor Y693F could

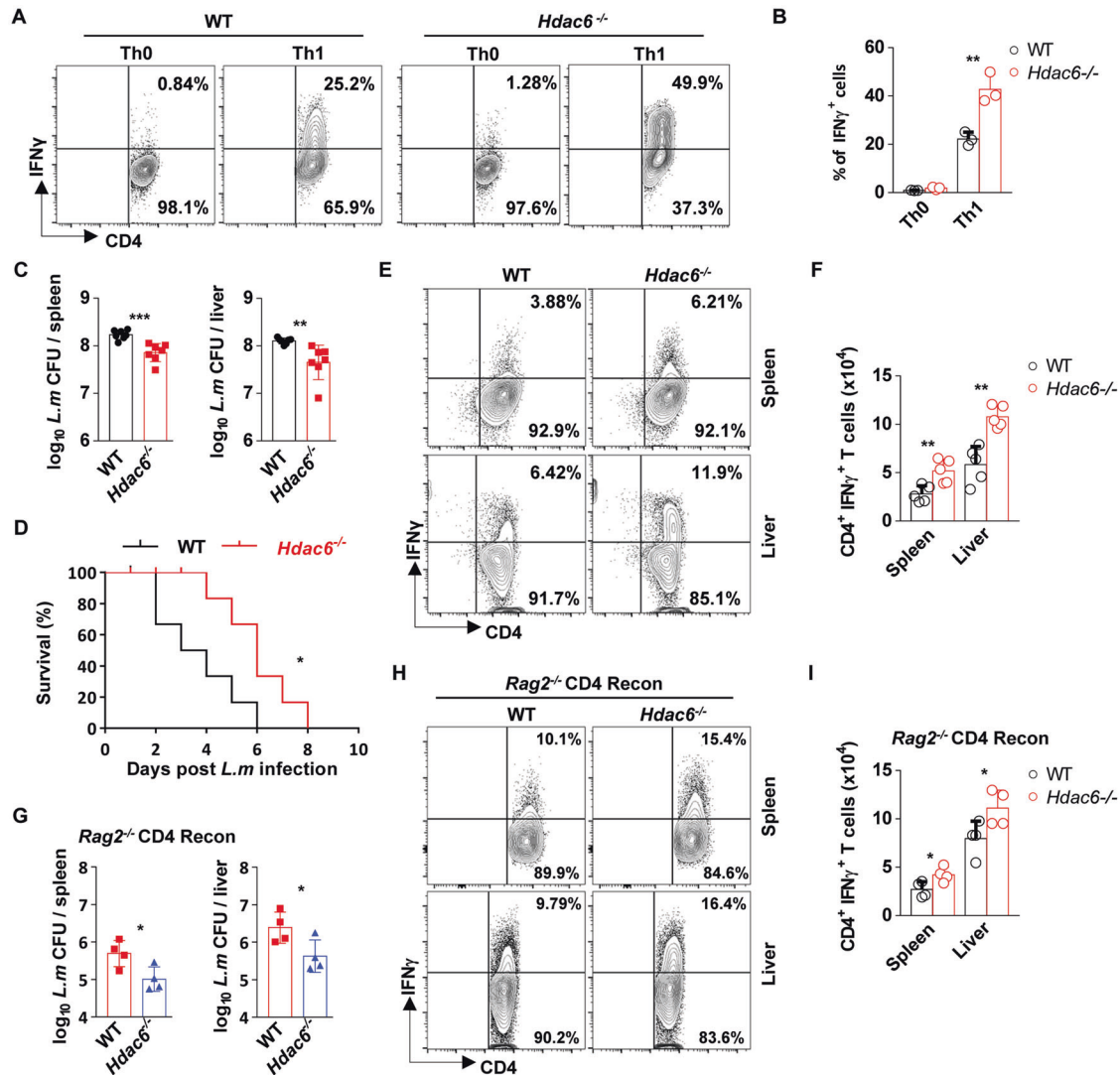


Fig. 2 *Hdac6*-deficient mice are resistant to *Listeria* infection. Representative FACS plots (A) and population frequencies (B) of Th1 cells polarized from wild-type (WT) or *Hdac6*^{-/-} naïve CD4⁺ T cells are shown. C *Listeria* CFUs per spleen (left) and liver (right) of WT and *Hdac6*^{-/-} mice infected with 1×10^4 *L. monocytogenes* i.v. ($n = 6$). D Survival rate of mice from Fig. 2C ($n = 7$). Representative FACS plots (E) and cell number (F) of CD4⁺ IFN γ ⁺ T cells in the spleen and liver of mice from Fig. 2C are shown. G *Listeria* CFUs per spleen (left) and liver (right) of infected *Rag2*^{-/-} mice reconstituted with either PBS or WT or *Hdac6*^{-/-} naïve CD4⁺ T cells ($n = 4$). Reconstituted *Rag2*^{-/-} mice were infected with 1×10^4 *Listeria* and sacrificed on day 5 for further analysis. Recon: reconstitution. Representative FACS plots (H) and cell number (I) of CD4⁺ IFN γ ⁺ T cells in the spleen and liver of mice from Fig. 2G are shown. The data are shown as the mean \pm SD of three independent experiments. * $p < 0.05$, ** $p < 0.01$ and *** $p < 0.001$, n.s means not significant (Student's *t* test).

rescue Th1 cell differentiation; however, the gain-of-function mutant STAT4-K667A partially rescued Th1 cell differentiation, as did WT STAT4 (Fig. 4I, J). STAT4-K673R and K691R possessed the ability to maintain Th1 differentiation (Fig. 4A, K). Taken together, our results demonstrate that STAT4-K667 is a bona fide acetylation site, which is important for STAT4 functionality.

STAT4-K667 acetylation is necessary for Y693 phosphorylation and STAT4 nuclear translocation

We further delineated the relationship between K667 acetylation and Y693 phosphorylation to investigate the mechanism by which acetylation of STAT4-K667 regulates its function. STAT4-K667R abolished JAK2-catalyzed phosphorylation of Y693 (Fig. S5A). However, STAT4-Y693F displayed the same acetylation level as WT STAT4 (Fig. S5B). In the WT or mutant STAT4 stable-transfected A1.1 cell line, which is a mouse-derived helper T cell hybridoma, STAT4-K667R markedly decreased phosphorylation of STAT4-Y693 (Fig. 5A). The acetylation mimic mutants K667Q (glutamine) and

K667A partially rescued STAT4 phosphorylation intensity (Fig. 5B). Consistently, WT HDAC6 substantially decreased STAT4 phosphorylation intensity, while HDAC6-H611A had no such effect (Fig. 5C). In primary CD4⁺ T cells, knockdown of CBP resulted in decreased phosphorylation levels of STAT4-Y693 (Fig. 5D). Both HDAC6 knockdown and depletion in CD4⁺ T cells increased STAT4-K667 acetylation and STAT4-Y693 phosphorylation (Fig. 5E–G). In *Listeria*-infected mice, HDAC6 inhibitors obviously enhanced the STAT4-K667 acetylation intensity (Fig. 5H). These data suggest that there is crosstalk between STAT4-K667 acetylation and STAT4-Y693 phosphorylation.

Interestingly, we found that compared with the binding between JAK2 and WT STAT4, the interaction between JAK2 and STAT4-K667R was dramatically reduced (Fig. 5I), indicating that K667 acetylation is required for JAK2-STAT4 complex formation. With immunofluorescence assay, we found that the intensity of phosphorylated STAT4 decreased obviously, and STAT4-K667R protein exhibited less sharp accumulation in the nucleus of IL-12-

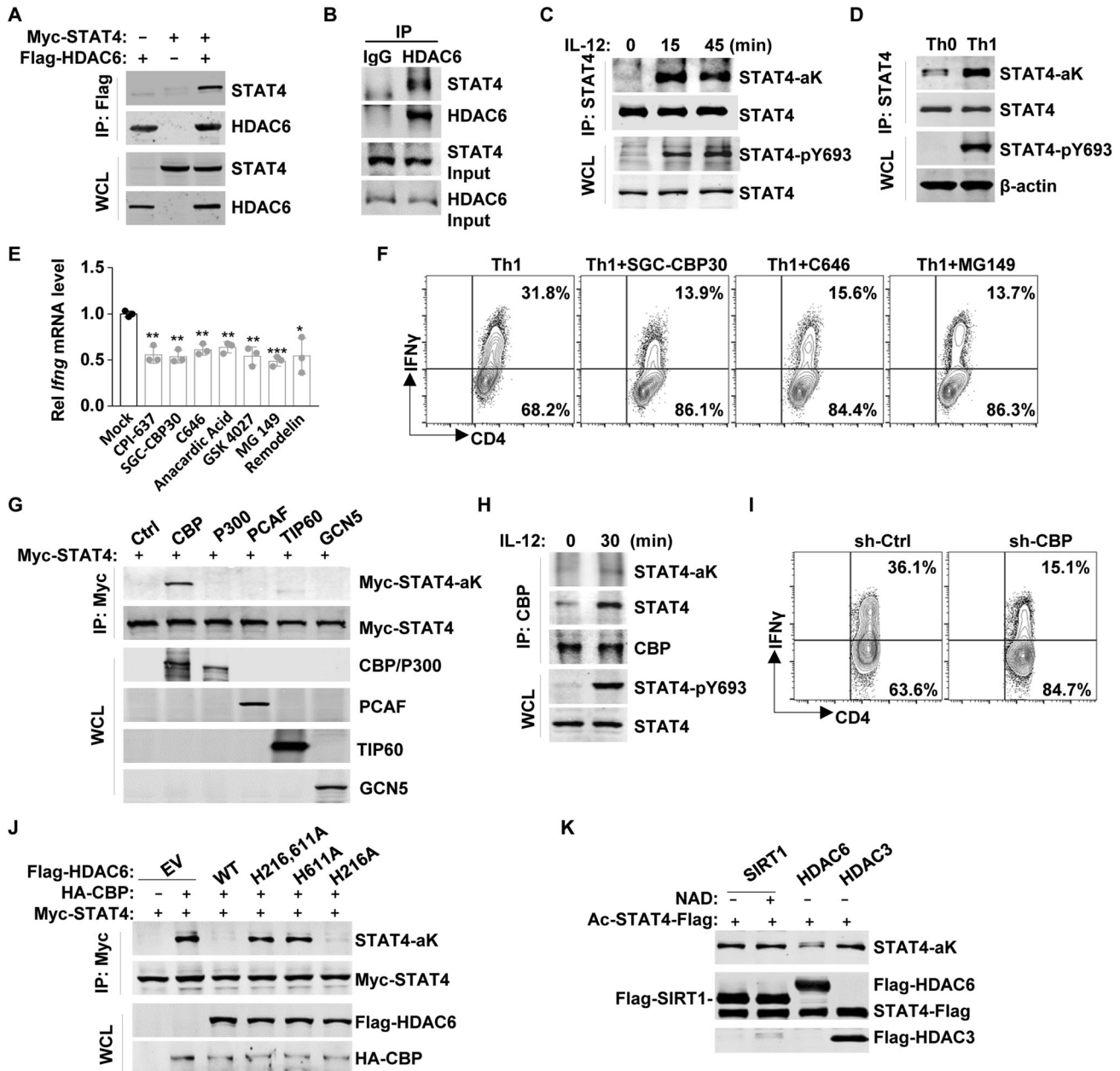


Fig. 3 HDAC6 and CBP reversibly modify the acetylation of STAT4. Coimmunoprecipitation (CoIP) and immunoblot analysis of HEK293T cells (A) transfected with the indicated constructs or primary CD4⁺ T cells (B). Immunoblot analysis of IL-12-treated CD4⁺ T cells (C) or polarized CD4⁺ T cells (D) after immunoprecipitation with an anti-STAT4 antibody. E qPCR analysis of the mRNA level of *Ifng* in CD4⁺ T cells on day 3 of induction into Th1 cell subsets in the absence or presence of HATs inhibitors. F Representative FACS plots of Th1 cells polarized in the presence or absence of HATs inhibitors are shown. G Immunoblot analysis of HEK293T cells transfected with the indicated constructs followed by immunoprecipitation with an anti-myc antibody. H CoIP and immunoblot analysis of primary CD4⁺ T cells treated with or without IL-12. I Representative FACS plots of Th1 cells polarized from CBP-knockdown and control naïve CD4⁺ T cells are shown. J Immunoblot analysis of STAT4 acetylation in HEK293T cells transfected with the indicated constructs. K Immunoblot analysis of STAT4 acetylation incubated in an in vitro system. The data are representative of three independent experiments with similar results or shown as the mean ± SD of three independent experiments. **p* < 0.05, ***p* < 0.01 and ****p* < 0.001 (Student's *t* test).

treated *Stat4*^{K667R} CD4⁺ T cells compared with that in IL-12-treated WT CD4⁺ T cells (Fig. 5J). It has been reported that leukemia inhibitory factor (LIF) and IFN α can induce STAT4-Y693 phosphorylation and activation [16–18]. Here, we found that the STAT4-K667R also exhibited reduced phosphorylation intensity and nuclear translocation in LIF- or IFN α -treated HeLa cells (Fig. S5C, D). Meanwhile, STAT4-K667R displayed a low level of transcriptional activity; however, the K667Q and K667A mutants partially rescued STAT4 transcriptional activity (Fig. 5K). HDAC6 substantially decreased the transcriptional activity of STAT4, while HDAC6-

H611A exhibited a much weaker effect on the transcriptional activity of STAT4 (Fig. 5L). Collectively, these results demonstrated that acetylation of STAT4-K667 is required for its interaction with JAK2, which safeguards the subsequent phosphorylation of Y693, nuclear translocation and transcription activity.

***Stat4*^{K667R} mice display impaired Th1 cell differentiation and low expression of Th1 cell polarization-related genes**

We further generated *Stat4*^{K667R} mice with the crisp/cas9 system (Fig. S6A). The frequencies of CD4⁺ and CD8⁺ T cells were similar

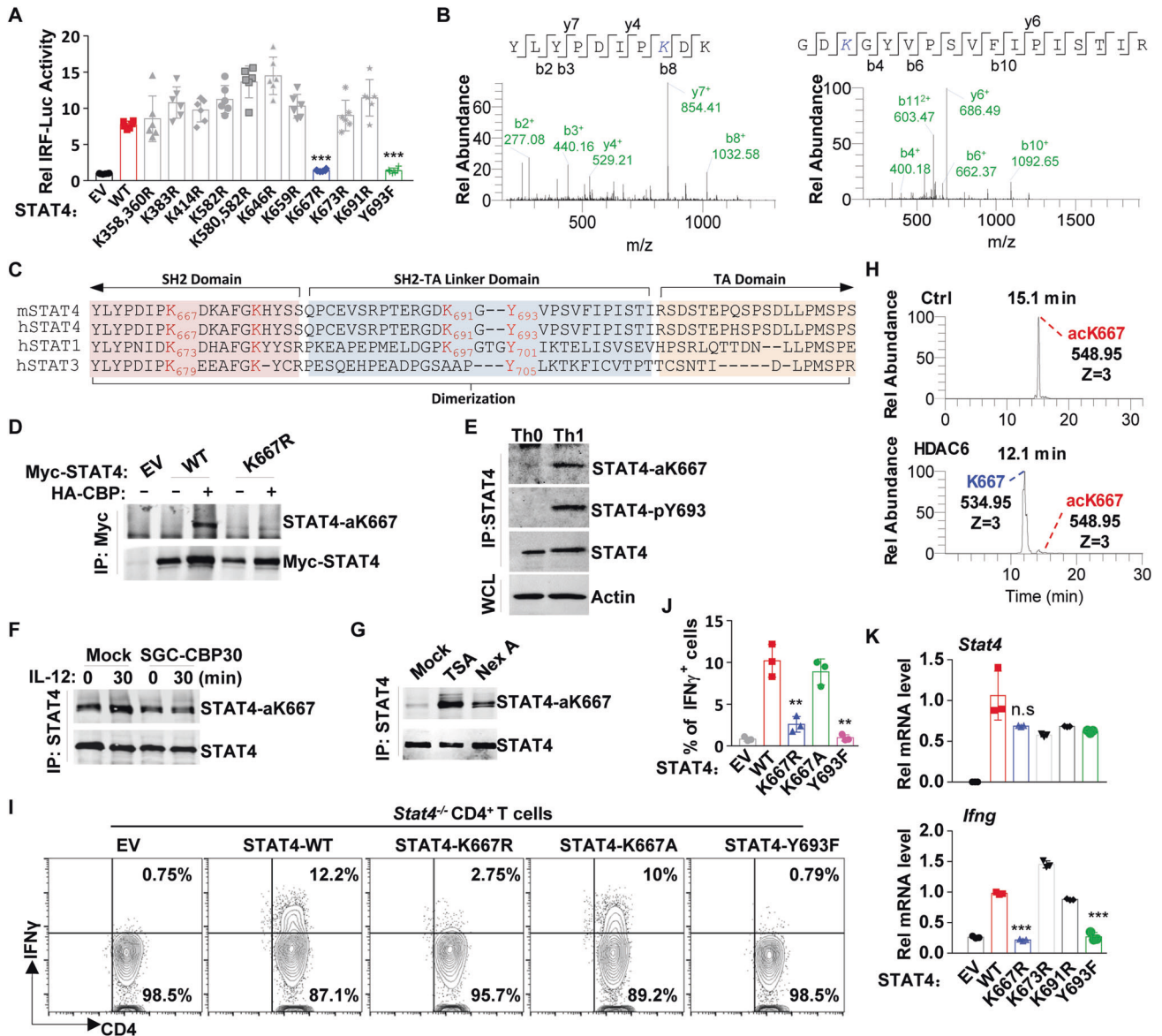


Fig. 4 Acetylation of STAT4-K667 is required for Th1 cell differentiation. **A** The IRF-luciferase reporter activity assay was performed in HEK293T cells transfected with empty vector (EV), WT or mutant STAT4 constructs. **B** Mass spectrometry analysis of purified STAT4 protein revealed the acetylation of STAT4 at two lysine residues. **C** Sequence alignment showing that the acetylated lysine residue 667 of STAT4 is conserved in both humans and mice species, as well as in the STAT protein family. **D** Immunoblot analysis of STAT4-K667 acetylation in HEK293T cells transfected with the indicated constructs. **E** Immunoblot analysis of polarized CD4⁺ T cells after immunoprecipitation with an anti-STAT4 antibody. **F** Immunoblot analysis of STAT4-K667 acetylation in CD4⁺ T cells pretreated with PBS or SGC-CBP30 (1 μ M) for 12 h followed by IL-12 treatment or not. **G** Immunoblot analysis of STAT4-K667 acetylation in CD4⁺ T cells primed into Th1 cells in the absence or presence of the indicated inhibitors. **H** Mass spectrometry analysis of acetylated STAT4-K667 peptide which were incubated with HDAC6 or not under in vitro system. **I, J** Representative FACS plots (**I**) and population frequencies (**J**) of Th1 cells polarized from naïve *Stat4*^{-/-} CD4⁺ T cells reconstituted with WT or mutant STAT4 are shown. **K** qPCR analysis of the mRNA levels of *Stat4* (upper) and *Ifng* (lower) in naïve *Stat4*^{-/-} CD4⁺ T cells reconstituted with WT or mutant STAT4, which were induced to differentiate into Th1 cells. The data are representative of three independent experiments with similar results or shown as the mean \pm SD of three independent experiments. ***p* < 0.01 and ****p* < 0.001, n.s means not significant (Student's *t* test).

under homeostatic conditions in the peripheral lymph organs of WT and *Stat4*^{K667R} mice (Fig. S6B, C). *Stat4*^{K667R} and *Stat4*^{-/-} CD4⁺ T cells comparably lost the ability to differentiate into Th1 cells compared with WT CD4⁺ T cells (Fig. 6A, B). However, STAT4-K667R did not affect Th17 cell and Treg cell differentiation (Fig. S6D).

By interrogating the gene expression signatures of WT, *Stat4*^{-/-} and *Stat4*^{K667R} Th0 and Th1 cells, we determined that in *Stat4*^{K667R} Th0 cells, the expression of Th1 cell marker genes *Ifng*, *Tbx21*, *Il12rb2* and genes associated with T cell cytotoxicity

(*Prf1* and *Nkg7*) significantly decreased, while the transcriptome profiles were quite similar between WT and *Stat4*^{-/-} Th0 cells (Fig. S6E–G). Gene set enrichment analysis (GSEA) revealed that the IL-12-mediated signaling pathway was substantially down-regulated in *Stat4*^{K667R} Th0 cells (Fig. S6H). Both hierarchical correlation clustering analysis and principal component analysis (PCA) showed different gene expression signatures in wild-type, *Stat4*^{-/-} and *Stat4*^{K667R} Th0 and Th1 cells (Fig. S6I, J). The expression levels of *Ifng* and *Tbx21* decreased more significantly in both *Stat4*^{K667R} and *Stat4*^{-/-} Th1 cells than in WT Th1 cells

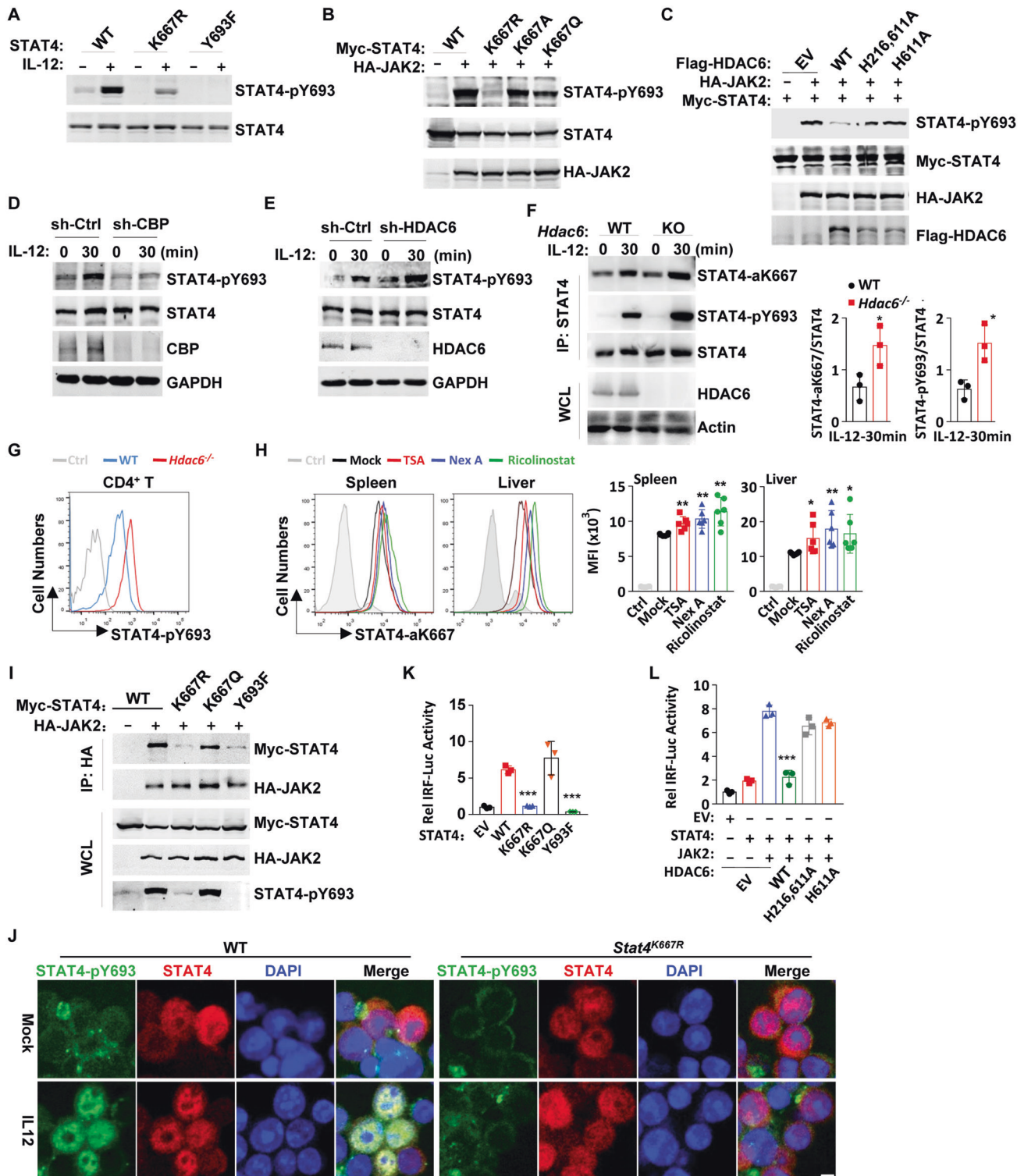


Fig. 5 Acetylation of STAT4-K667 is required for phosphorylation of Y693 and STAT4 nuclear translocation. **A** Immunoblot analysis of STAT4-Y693 phosphorylation levels in A1.1 cells stably transfected with STAT4-constructs treated with or without IL-12. **B, C** Immunoblot analysis of STAT4-Y693 phosphorylation levels in HEK 293 T cells transfected with the indicated constructs. Immunoblot analysis of STAT4-Y693 phosphorylation levels in control or CBP-knockdown (**D**) or HDAC6-knockdown (**E**) CD4⁺ T cells treated with IL-12 or not. **F** Left, immunoblot analysis of STAT4 acetylation and phosphorylation levels in WT or HDAC6-deficient CD4⁺ T cells treated with or without IL-12. Right, quantification of the relative modified STAT4 level from three independent experiments. **G** Mean flour intensity of phosphorylated STAT4-Y693 in WT and *Hdac6*^{-/-} naïve CD4⁺ T cells on day 4 of induction into Th1 cell subsets. **H** Mean flour intensity of acetylated STAT4-K667 in CD4⁺ T cells from the spleen and liver of mice from Fig. 1E. **I** CoIP and immunoblot analysis of HEK293T cells transfected with the indicated constructs. **J** Immunofluorescence analysis of CD4⁺ T cells from WT or *Stat4*^{K667R} mice treated with or without IL-12 for 30 min. Scale bar, 50 μm. **K, L** The IRF-luciferase reporter activity assay was performed in HEK 293 T cells transfected with the indicated constructs. The data are representative of three independent experiments with similar results or shown as the mean ± SD of three independent experiments. **p* < 0.05, ***p* < 0.01 and ****p* < 0.001 (Student's *t* test).

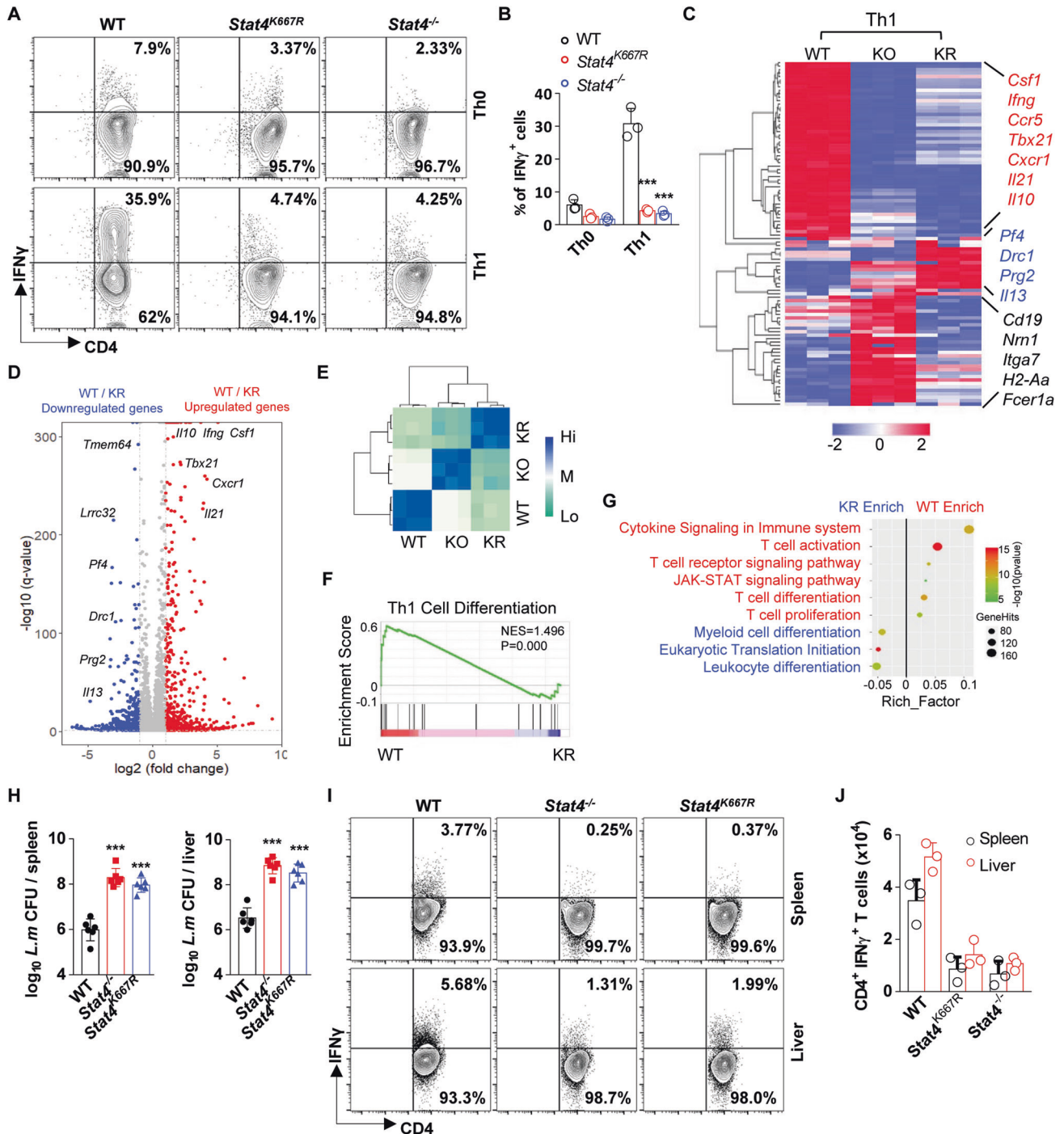


Fig. 6 *Stat4*^{K667R} mice display impaired Th1 cell differentiation and are more susceptible to *Listeria* infection. Representative FACS plots (A) and population frequencies (B) of Th1 cells polarized from WT, *Stat4*^{K667R} or *Stat4*^{-/-} naïve CD4⁺ T cells are shown. C Top 100 differentially expressed genes from RNA-seq among WT, KO (*Stat4*^{-/-}) and KR (*Stat4*^{K667R}) Th1 cells. D Volcano plot of significantly altered genes between WT and KR Th1 cells. E Hierarchical clustering of Pearson correlations of DESeq2 normalized counts for the RNA-seq libraries among WT, KO and KR Th1 cells. Colors represent the Pearson correlation coefficient. F GSEA plots of KR Th1 cells show downregulation of Th1 cell differentiation. G GO analysis of WT and KR Th1 cells for the top differentially regulated gene sets. H *Listeria* CFUs per spleen (left) and liver (right) of WT, *Stat4*^{-/-} and *Stat4*^{K667R} mice infected with 1 × 10⁴ *L. monocytogenes* (n = 6). Representative FACS plots (I) and cell number (J) of CD4⁺ IFN γ ⁺ T cells in the spleen and liver of mice from Fig. 6H are shown. The data are representative of three independent experiments with similar results or shown as the mean ± SD of three independent experiments. ***p < 0.001 (Student's t test).

(Fig. 6C, D). Consistently, hierarchical correlation clustering analysis showed an obvious correlation between *Stat4*^{K667R} and *Stat4*^{-/-} Th1 cells, which separately clustered from WT Th1 cells (Fig. 6E). GSEA and GO analysis revealed that the genes downregulated in *Stat4*^{K667R} cells were enriched in Th1 cell

differentiation, cytokine signaling and the JAK-STAT signaling pathway (Fig. 6F, G). Genes related to T cell activation and proliferation were also downregulated in *Stat4*^{K667R} Th1 cells (Fig. 6G). Within the CD4⁺ T cell compartment from both the spleen and lymph nodes, we observed a significant decrease in

the proportion of effector and memory cells (CD62L^{low} CD44^{high}) and proliferative Ki67⁺ cells in *Stat4*^{K667R} CD4⁺ T cells (Fig. S6I, J). Between the WT and *Stat4*^{K667R} CD8⁺ T cell compartments, however, we noticed less obvious differences in the proportions of effector and memory cells and proliferating cells (Fig. S6K, L). However, T cell proliferation inhibitory genes and myeloid differentiation signaling effectors, such as proteoglycan (*Prg2*), leucine rich repeat containing 32 (*Lrrc32*), and platelet factor 4 (*Pf4*), were upregulated in *Stat4*^{K667R} Th1 cells (Fig. 6D, G).

Together, these data indicate that acetylation of STAT4-K667 is required for the expression of Th1 cell differentiation-related genes.

ChIP-Seq analysis revealed STAT4 binding in the promoter of Th1 cell polarization-related genes

We noticed that the expression of Th1 cell polarization-related genes consistently decreased in *Stat4*^{-/-} and *Stat4*^{K667R} Th1 cells (Fig. S7A), suggesting that the expression of those genes was dependent on STAT4-K667 acetylation. qPCR analysis confirmed a reduction in the STAT4 acetylation-dependent genes (Fig. S7B). Analysis of publicly available chromatin immunoprecipitation (ChIP)-seq data from polarized WT and *Stat4*^{-/-} Th1 cells [19], revealed a strong enrichment of STAT4 occupancy in the promoter/enhancer regions of *Ifng*, *Ccl4*, *Csf1* and so on (Fig. S7C), and STAT4 deficiency resulted in a significant reduction in H3K4me3 and H3K4me1 marks (Fig. S7D) [20, 21]. On the other hand, we analyzed the publicly available data of the assay for transposase-accessible chromatin using sequencing (ATAC-seq) from WT and *Stat4*^{-/-} T follicular helper (Tfh) cells, which are a functionally and phenotypically distinct subset of CD4⁺ Th cells that produce the cytokines IL-21 and IFN γ [22]. The results showed that the chromatin accessibility in the promoters and proximal enhancers of the genes *Ccl4*, *Tbx21*, *Lag3* and *Ifng* revealed no significant differences between WT and *Stat4*^{-/-} Tfh cells (Fig. S7E). We proposed that neither STAT4 deficiency nor STAT4-K667R mutation would affect the accessible chromatin landscape of Th1 cell differentiation-related genes. With ChIP-qPCR, we found that STAT4-K667R displayed less occupancy on the promoters of *Ifng*, *Ccl4* and *Csf1* (Fig. S7F). These findings suggested that acetylation of K667 promoted STAT4 targeting of Th1 cell differentiation-related genes.

Stat4^{K667R} mice are more susceptible to *Listeria* infection

In *Listeria* infection model, *Stat4*^{-/-} mice showed dramatically increased bacterial burdens in the spleen and liver and a significantly decreased survival rate compared with WT mice; however, the disease severity of *Stat4*^{K667R} mice was slightly milder than that of *Stat4*^{-/-} mice but was more severe than WT mice (Fig. 6H and S8A). The percentage of Th1 cells from the spleen and liver of both *Stat4*^{K667R} and *Stat4*^{-/-} mice was significantly less than the amount of Th1 cells from the WT group (Fig. 6I, J). The expression of chemokines and proinflammatory cytokines was comparably increased between IFN γ -treated WT and *Stat4*^{K667R} BMDMs compared with untreated control cells (Fig. S8B). These results suggest that acetylation of STAT4-K667 plays a critical role in maintaining Th1 cell-mediated immunity against *Listeria* infection.

HDAC6 inhibitors reduce *Listeria* infection in a STAT4-K667-dependent manner

We further found that the inhibitors TSA, Nex A and ricolinostat significantly promoted Th1 cell differentiation in WT CD4⁺ T cells but not in *Stat4*^{K667R} CD4⁺ T cells (Fig. 7A–C). Meanwhile, the infection-preventing effect of HDAC6 inhibitors only existed in WT mice but not in *Stat4*^{-/-} or *Stat4*^{K667R} mice (Fig. 7D), indicating that the protective effect of HDAC6 inhibitors in *Listeria* infection was dependent on STAT4-K667.

Taken together, the study proved that by promoting STAT4-K667 acetylation with HDAC6 inhibitors, Th1 cells accumulated significantly in the mouse spleen and liver, which effectively ameliorated *L. monocytogenes* infection in mice (Fig. 7E).

DISCUSSION

In this study, we aimed to identify new pharmacological molecules involved in the Th1 cell differentiation process. We found that ricolinostat and Nex A dramatically elevated Th1 cell differentiation and significantly ameliorated *Listeria*-burden in mice by inhibiting HDAC6 enzymatic activity and decreasing the acetylation level of STAT4. Moreover, *Hdac6*^{-/-} mice exhibited more potential for Th1 cell development and were more resistant to *Listeria* infection than WT mice. Mice with defects in STAT4 acetylation failed to upregulate Th1 cell polarization and developed more severe *Listeria* infection. Our study highlights an important yet previously unappreciated role of HDAC6 in orchestrating Th1 cell differentiation and the related antibacterial response.

Mechanistically, CBP catalyzed the acetylation of STAT4-K667 in Th1 cells, which is located in the SH2 domain. The SH2 domain of STAT is composed of “ $\alpha\beta\beta\beta\alpha$ ” motifs discrete with positive lysine residues. The acetylation of these lysine residues may therefore remodel the conformation of the SH2 domain to enable it to form a complex with phosphorylated tyrosine. We identified that the binding between STAT4-K667R and JAK2 decreased significantly, which explains why STAT4-K667R blocked phosphorylation of STAT4-Y693. The transcriptomes of WT, *Stat4*^{-/-} and *Stat4*^{K667R} Th0 and Th1 cells revealed that most Th1 cell differentiation-related genes were largely dependent on STAT4-K667 acetylation for their expression. This study identifies that STAT4 acetylation positively regulates STAT4 activity and primes Th1 cell development.

In the classical dichotomy hematopoiesis model, T cells and B cells arise from common lymphoid progenitors, while macrophages, neutrophils and other leukocytes arise from common myeloid progenitors. However, several studies have reported that T cell progenitors retain substantial B cell and myeloid potential in the adult thymus [23, 24]. Intriguingly, we noticed that the genes involved in the positive regulation of B cell activation, macrophage activation and monocyte chemotaxis and neutrophil chemotaxis were significantly upregulated in *Stat4*^{K667R} CD4⁺ T cells (Fig. S6E, F). We speculate that STAT4-K667R might play a role in sustaining the myeloid potential of T cells in peripheral lymphoid organs.

CD8⁺ T cells are supposed to be the main T cells involved in the clearance of intracellular pathogens with cytotoxicity; however, we found that ricolinostat and Nex A exerted less significant effects on IFN γ -secreting CD8⁺ T cells. HDAC6 protein was expressed at the same level in both CD4⁺ and CD8⁺ T cells (data not shown). We excluded the possibility that the differential effects of HDAC6 on CD4⁺ and CD8⁺ T cells were caused by differential expression levels of HDAC6. Although IL-12 can augment both CD4⁺ and CD8⁺ T cells to secrete IFN γ during intracellular infection, the mechanisms involved in the two processes are quite different. In CD4⁺ T cells, IL-12-activated STAT4 is the key for Th1 cell differentiation and IFN γ secretion. However, it has been reported that in CD8⁺ T cells, the IL-12-mediated increase in IFN γ secretion is due to increased MAPKs and AKT activation and T-bet expression but not due to STAT4 activation [25–27]. Thus, we suggest that the reason HDAC6 shows less regulation of CD8⁺ T cells during *Listeria* infection is that HDAC6's downstream substrate STAT4 displays a minor regulatory effect on CD8⁺ T cell function.

L. monocytogenes is a food-borne bacterium that causes listeriosis. Since listeriosis occurs more frequently in immunocompromised individuals and pregnant women, exploring new

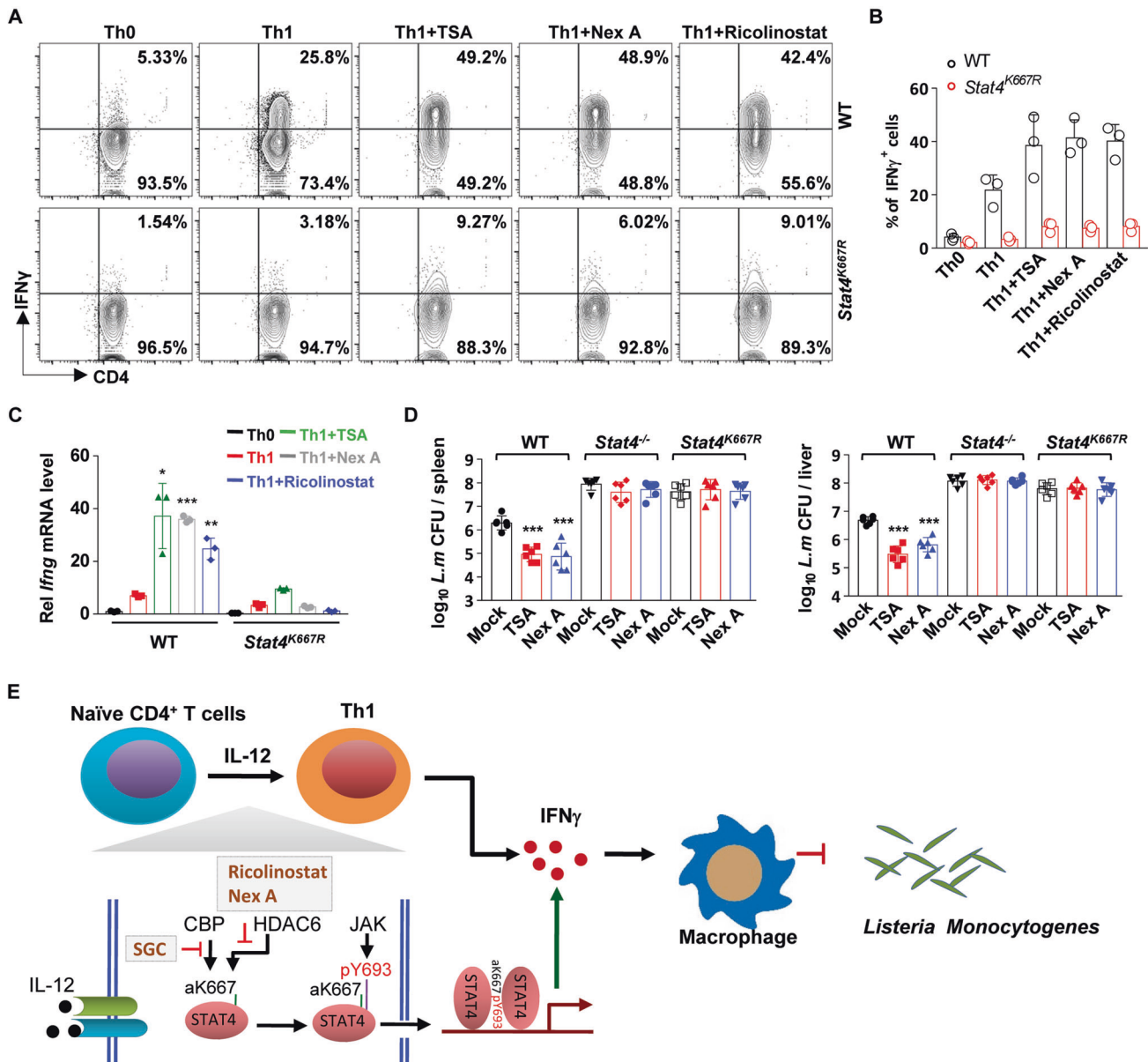


Fig. 7 HDAC6 inhibitors reduce *Listeria* infection in a STAT4-K667 dependent manner. Representative FACS plots (A) and population frequencies (B) of Th1 cells polarized from WT or Stat4^{K667R} naïve CD4⁺ T cells are shown. WT or Stat4^{K667R} naïve CD4⁺ T cells were cultured in the absence or presence of HDACs inhibitors. C qPCR analysis of the mRNA level of *Ifng* in the CD4⁺ T cells from Fig. 7A. D *Listeria* CFUs per spleen (left) and liver (right) of WT, Stat4^{-/-} and Stat4^{K667R} mice infected with *L. monocytogenes* i.v. and treated with vehicle saline, TSA, Nex A or Ricolinostat accordingly i.p. (n = 6). E Schematic diagram of Th1 polarization induced by STAT4-K667 acetylation during *Listeria* infection. The data are representative of three independent experiments with similar results or shown as the mean \pm SD of three independent experiments. * $p < 0.05$, ** $p < 0.01$ and *** $p < 0.001$ (Student's *t* test).

strategies to enhance Th1 cell-mediated immunity is of obvious significance. Our study shows that the HDAC6 inhibitors ricolinostat and Nex A could directly promote Th1 cell differentiation by enhancing acetylation of STAT4-K667 and ameliorate the *L. monocytogenes* infection in mice. This mechanism may be targeted in human intracellular bacterial infection treatment, and ricolinostat and Nex A could serve as potential therapies for treating intracellular pathogen infection.

MATERIALS AND METHODS

Mice

Stat4^{-/-} and Rag2^{-/-} mice were purchased from Nanjing Biomedical Research Institute of Nanjing University, and back crossed to C57BL6 background. Stat4^{K667R} mutant mice were generated with the Crisp-cas9 system. Hdac6^{-/-}

mice were provided by the Yu Zhang laboratory from the National Institute of Biological Sciences, Beijing. Stat4^{-/-}, Stat4^{K667R}, Hdac6^{-/-}, Rag2^{-/-} and their representative wild-type control mice were maintained in a specific-pathogen-free (SPF) facility. 6–12 weeks old mice were used in all animal-related experiments. Age and sex matched mice were used in all animal-related experiments.

Culture and maintenance of cell lines

HEK293T, NIH 3T3 and Plat E cell lines were cultured in DMEM (HyClone) supplemented with 10% fetal bovine serum (Genmini), 100 units/ml penicillin, and 100 μ g/ml streptomycin (Shenggong). A1.1 cell line was cultured in RPMI (HyClone) supplemented with 10% fetal bovine serum (Genmini), 100 units/ml penicillin, and 100 μ g/ml streptomycin (Shenggong). All cell lines were purchased from the Cell Bank of the Chinese Academy of Sciences and routinely tested for mycoplasma contamination with PCR.

In vitro T cell culture

Spleens and lymph nodes were collected from mice of different genotypes, and single-cell suspensions were prepared by mechanical disruption in PBS. Naïve CD4⁺ T cells were isolated by magnetic sorting with a Miltenyi Biotec CD4⁺ CD62L⁺ T Cell Isolation kit, according to the manufacturer's directions (Miltenyi Biotec, 130-106-643). CD4⁺ T cells were cultured in IMDM (HyClone) supplemented with 10% FBS (Genmini), 100 units/ml penicillin, 100 µg/ml streptomycin (Shengong), 4 mM L-glutamine, and 50 µM β-mercaptoethanol, and activated with 5 µg/ml precoated anti-CD3 (eBioscience) and 2 µg/ml anti-CD28 (eBioscience). Th1 cells were differentiated by the addition of recombinant IL-12 (1 ng/ml, R&D Systems) and anti-IL-4 (10 µg/ml, BD Pharmingen). Th17 cells were differentiated by the addition of recombinant IL-6 (20 ng/ml, R&D Systems), recombinant TGF-β (1 ng/ml, R&D Systems), anti-IFNγ (10 µg/ml, BD Pharmingen) and anti-IL-4 (10 µg/ml, BD Pharmingen), followed by recombinant IL-23 (30 ng/ml, R&D Systems) on day 3. Treg cells were differentiated by the addition of TGF-β (5 ng/ml, R&D Systems) and recombinant IL-2 (40 ng/ml, PeproTech). CD4⁺ T cell cultures were split at a ratio of 1:2 on day 3 after activation.

Flow cytometry

Single cell suspensions were pelleted, resuspended and stained with Live/Dead-violet (Life Technologies) in PBS for 30 min on ice. Cells were washed and resuspended with surface-staining antibodies in PBS supplemented with 1% FBS. For transcription factor staining, cells were fixed and permeabilized with the FoxP3 staining buffer set from eBioscience according to the manufacturer's protocol. Intracellular stains were prepared in 1X eBioscience permwash buffer containing conjugated antibodies. Staining was performed for 30–60 min on ice. For cytokine analysis, CD4⁺ or CD8⁺ T cells were activated for 4–5 h with PMA (50 ng/ml, Sigma) and ionomycin (500 ng/ml, Sigma), and Golgi Stop (BD Pharmingen) was added. After live/dead and surface staining, cells were treated with the Cytofix/Cytoperm solution set (BD Pharmingen) according to the manufacturer's protocol. Intracellular stains were prepared in BD permwash. Absolute numbers of isolated cells from peripheral mouse tissues in all studies were determined by comparing the ratio of cell events to bead events of CountBright absolute counting beads. Samples were acquired on a Gallios (Beckman Coulter), and the data were analyzed with FlowJo software.

Epigenetic compound library screening

96-round-bottom well plates were coated with anti-CD3 antibody overnight at 4 °C. Naïve CD4⁺ T cells were isolated and primed into the Th1 cell subtype as described in the in vitro T cell culture section. A compound library of 188 chemicals targeting different epigenetic modifiers. Each compound in the epigenetic compound library (MCE) was diluted to 0.02 to 10 µM accordingly in IMDM medium. Naïve CD4⁺ T cells were treated with each compound or untreated from the scratch while they were cultured in Th1 cell conditions. The cells were collected 72 h later by centrifugation at 300 × g for 5 min, washed with PBS, and then treated with the Turbo Capture 96 mRNA Kit (Qiagen, 72251) following the manufacturer's instructions. The cell lysates from each well were collected for qRT-PCR using the Hifair® II 1st Strand cDNA Synthesis Kit (Yeasten, 11121ES60), following the manufacturer's instructions. Each compound was tested in triplicate.

RNA isolation and cDNA preparation

Total RNA from in vitro polarized T cells was extracted using TRIzol (Invitrogen) followed by DNase I (Qiagen) treatment and cleanup with the RNeasy MiniElute kit (Qiagen) following the manufacturer's protocols. cDNA was generated using the Hifair® II 1st Strand cDNA Synthesis Kit (Yeasten, 11121ES60).

qRT-PCR

Quantitative RT-PCR was performed using the Hieff® qPCR SYBR Green Master Mix (Low Rox Plus) (Yeasten, 11202ES08) on the Real-Time PCR System (ABI QuantStudio™ 7 Flex). Gene specific primers spanning exons were used. Values were normalized to β-actin for each sample. 'Fold differences' were calculated with the ΔΔC_t method.

Whole cell extraction, immunoprecipitation and western blot analysis

Cells were collected and lysed in ice-cold RIPA buffer (Millipore, 20–188) containing inhibitors (1 mM phenylmethylsulfonyl fluoride, cocktails of protease inhibitors, 1 mM Na₃VO₄, 1 mM NaF). Cell debris was removed by

centrifugation at 4 °C, 13,000 r.p.m. for 15 min. The cell supernatants were subjected to immunoprecipitation using the appropriate antibodies and protein A or protein G-Sepharose beads. Protein extracts were analyzed by SDS-PAGE and immunoblotting with the indicated antibodies. The following primary antibodies were commercially obtained: acetylated-lysine (9441; Cell Signaling Transduction), Stat4 pY693 (554002; BD Biosciences), Stat4 (sc-398228; Santa Cruz), Myc, HA, Flag (F7425; Sigma-Aldrich), CBP, HDAC6 (sc-5258; Santa Cruz), actin and Gapdh. A polyclonal antibody against acetyl-lysine 667 STAT4 was generated by immunizing rabbits at Ab land company. Primary antibodies were visualized using corresponding secondary a-mouse or a-rabbit Dylight 800/680 antibodies (Li-COR) and signal intensities were quantified using the Li-COR Odyssey Infrared Imaging system. All of the full length original western blots for these results are provide in Supplementary File 1.

Luciferase reporter assay

HEK293T or NIH 3T3 cells were plated in 48-well plates and transfected with a DNA mixture containing 0.2 µg of 2x-IRF-luciferase reporter plasmid (Promega, pGL3-basic), 2 ng of a plasmid containing *Renilla* luciferase (Promega, pRL-CMV), and 0.2 µg of STAT4 constructs. Transfection was performed using Lipofectamine 2000 (Invitrogen) according to the manufacturer's instructions. Chemical inhibitors or vehicle control was added 36 h after transfection and luciferase activity was measured 8 h later using a dual-luciferase reporter kit (Promega).

In vitro deacetylation assay

An in vitro deacetylation assay was performed as described previously [28]. Briefly, the Flag-SIRT1, Flag-HDAC6 and Flag-HDAC3 constructs were expressed in HEK293T cells individually. The proteins were purified with M2 beads and eluted with Flag peptide. STAT4-Flag and CBP constructs were coexpressed in HEK293T cells at a ratio of 1:5. Acetylated STAT4 was purified with M2 beads and eluted with Flag peptide. A total of 1 µg of the purified SIRT1, HDAC6 or HDAC3 was incubated with 1 µg of purified ac-STAT4 in reaction buffer (10 mM Tris-HCl, pH 8.0, 150 mM NaCl, 1 mM MgCl₂, 10% glycerol and protease inhibitor cocktail) with or without NAD at 30 °C for 1 h. Samples were analyzed by western blot.

A total of 100 ng of acetylated-STAT4 K667 peptide (PDIPK_{ac}/DKAFG-KHYS) was incubated with or without 1 µg of purified HDAC6 in the above reaction buffer at 30 °C for 1 h. Samples were desalted using C18 Zip Tips and were then subjected to LC-mass spectrometry for analysis.

Mass spectrometric analysis of lysine acetylation

MS analysis was performed as described previously ([16]). In brief, Myc-tagged STAT4 constructs of mouse origin and CBP constructs were transfected into HEK293T cells that were cultured in 10-cm Petri dishes using Lipofectamine 2000. Twenty-four hours later, the cells from two dishes were collected to immunoprecipitate STAT4 with 2 µg of anti-myc antibody and protein G agarose beads. The immunoprecipitated STAT4 from the above HEK293T cells was separated via SDS-PAGE. The Coomassie blue-stained STAT4 band was excised from the gel for protease digestion followed by liquid chromatography-tandem mass spectrometric analysis with a Thermo LC-MS/MS system. The spectra from MS were analyzed with Protein Discovery software (version 2.2).

Retrovirus package and reconstitution of T cells

Plat E cells were seeded into 10-cm petri dishes and transfected with a DNA mixture containing 21 µg of wild-type or mutant STAT4 plasmids (pMSCV-PIG-puro) and 3 µg of pCL-eco plasmid to generate retrovirus. 24 h later, the cell media were collected and filtered. Naïve CD4⁺ T cells were seeded into anti-CD3 precoated 48-well plates and cultured under Th1 cell differentiation conditions. 16 h after anti-CD3/28 activation, CD4⁺ T cell media were removed, and media containing retrovirus was gently added to CD4⁺ T cells. The 48-well plate was centrifuged at 900 g and 37 °C for 90 min. 4 h later, media containing retrovirus was discarded, and Th1 cell conditioned media were added back to CD4⁺ T cells. The above procedure was repeated once 24 h later. Puromycin was used to eliminate uninfected cells. The CD4⁺ T cell phenotype was analyzed on day4 with flow cytometry and qRT-PCR.

RNA-sequencing and data analysis of T cells

Th0 and Th1 cells from wild-type, *Stat4*^{K667R} mutant or *Stat4*^{-/-} mice were cultured as described above. Total RNA from Th0 or Th1 cells was

extracted, cleaned up as described above and used for RNA-seq analysis. cDNA library construction and sequencing were performed by Beijing Novogene Corporation. Briefly, a total amount of 3 µg RNA per sample was used as input material for the RNA sample preparations. Sequence libraries were generated using the NEBNext UltraTM RNA Library Prep Kit for Illumina (NEB) following the manufacturer's instructions, and index codes were added to attribute sequences to each sample. The clustering of the index-coded samples was performed on a cBot Cluster Generation System using TruSeq PE Cluster Kit v3-cBot-HS (Illumina) according to the manufacturer's instructions. After cluster generation, the library preparations were sequenced on an Illumina HiSeq platform and 125 bp/150 bp paired-end reads were generated. We used featureCounts v1.5.0-p3 to count the reads numbers mapped to each gene. The FPKM of each gene was calculated based on the length of the gene and reads count mapped to this gene. Differential expression analysis of the two groups was performed using the DESeq2 R package (1.16.1). Heatmaps of gene expression were generated using the R language (version 3.2.1) and were generated on the basis of \log_2 (FPKM). Gene ontology (GO) enrichment analysis of differentially expressed genes was implemented using Gene Set Enrichment Analysis (GSEA; <http://www.broadinstitute.org/gsea/index.jsp>).

CUT&RUN

CUT&RUN experiments were carried out as described previously [29]. Briefly, 5×10^5 fresh cells were harvested, captured with concanavalin A-coated magnetic beads and incubated with anti-H3K27ac antibody or control IgG antibody overnight at 4 °C. After washing away the unbound antibody with Dig-wash buffer (20 mM HEPES-NaOH pH 7.5, 150 mM NaCl, 0.5 mM spermidine, 0.025% digitonin and 1x protease inhibitor cocktails), protein A-MNase was added and incubated for 1 h at 4 °C. After washing, CaCl_2 was added to each sample at a final concentration of 2 mM to activate protein A-MNase. The reaction was carried out in ice water bath for 30 min and stopped by addition of 2xSTOP buffer (340 mM NaCl, 20 mM EDTA, 4 mM EGTA, 0.05% digitonin, 100 µg/mL RNase A and 50 µg/mL glycogen). DNA was extracted with MinElute PCR Purification Kit (Qiagen, 28004).

L. monocytogenes infection and enumeration of bacterial load

The *L.monocytogenes* strain 10403 s (provided by Y. Qian, Institute of Health Sciences, Shanghai Institutes for Biological Sciences) was used in this study. *L. monocytogenes* were stored as glycerol stocks at -80 °C and cultured in brain heart infusion (BHI) broth containing 50 µg/ml streptomycin overnight at 37 °C with shaking. For infections, *L. monocytogenes* were grown to mid-log phase and then diluted into pyrogen-free PBS. Age- and sex-matched mice (8–10 weeks of age) were injected i.v. with 1×10^4 CFU of *L. monocytogenes* and killed on day 5. To determine organ *Listeria* burden, spleens and livers were homogenized separately in PBS. Serial dilutions of homogenate were plated on BHI agar plates, and *L. monocytogenes* CFUs were assessed after overnight growth at 37 °C.

CD4⁺ T cell reconstitution of *Rag2*^{-/-} mice

CD4⁺ T cell reconstitution of *Rag2*^{-/-} mice was carried out as described previously [29, 30]. Negatively isolated naïve CD4⁺ T cells were purified from the spleen and lymph nodes of WT or *Hdac6*^{-/-} mice as described in the in vitro T cell culture section. 2×10^5 CD4⁺ T cells were then injected into *Rag2*^{-/-} mice via tail vein injection. Mice were left for 8 weeks and then tested for the success of reconstitution by FACS staining of spleen and liver cell suspensions for the presence of CD4.

Quantification and statistical analysis

The statistical significance of comparisons between two groups was performed using a two-tailed, unpaired t test, * $p < 0.05$, ** $p < 0.01$ and *** $p < 0.001$, n.s means not significant (Student's t test). GraphPad Prism 7 software (GraphPad Software) was used to plot all the graphs and calculate statistical significance.

DATA AVAILABILITY

RNA-seq datasets are deposited in the Gene Expression Omnibus (GEO) with accession number GEO: GSE146253. We collected ChIP-seq and ATAC-seq data from the GEO public resource (<http://www.ncbi.nlm.nih.gov/geo>) and the accession numbers are GSM550303, GSM550304, GSM2828376, GSM2828377, GSM2828378,

GSM2828379, GSM836118, GSM836120, GSM994512, and GSM994513. All of the full length original western blots for these results are provide in Supplementary File 1.

REFERENCES

- Kaplan MH, Sun YL, Hoey T, Grusby MJ. Impaired IL-12 responses and enhanced development of Th2 cells in Stat4-deficient mice. *Nature* 1996;382:174–7.
- Thierfelder WE, van Deursen JM, Yamamoto K, Tripp RA, Sarawar SR, Carson RT, et al. Requirement for Stat4 in interleukin-12-mediated responses of natural killer and T cells. *Nature* 1996;382:171–4.
- Wagner RD, Steinberg H, Brown JF, Czuprynski CJ. Recombinant interleukin-12 enhances resistance of mice to *Listeria monocytogenes* infection. *Micro Pathogenesis*. 1994;17:175–86.
- Wieczorek M, Ginter T, Brand P, Heinzel T, Krämer OH. Acetylation modulates the STAT signaling code. *Cytokine Growth F R* 2012;23:293–305.
- Nijhuis L, Peeters JGC, Vastert SJ, van Loosdregt J. Restoring T Cell Tolerance, Exploring the Potential of Histone Deacetylase Inhibitors for the Treatment of Juvenile Idiopathic Arthritis. *Front Immunol*. 2019;10:151.
- Nusinzone I, Horvath CM. Positive and negative regulation of the innate antiviral response and beta interferon gene expression by deacetylation. *Mol Cell Biol*. 2006;26:3106–13.
- Into T, Inomata M, Niida S, Murakami Y, Shibata K-I. Regulation of MyD88 aggregation and the MyD88-dependent signaling pathway by sequestosome 1 and histone deacetylase 6. *The J Biol Chem*. 2010;285:35759–69.
- Kovacs JJ, Murphy PJM, Gaillard S, Zhao X, Wu J-T, Nicchitta CV, et al. HDAC6 regulates Hsp90 acetylation and chaperone-dependent activation of glucocorticoid receptor. *Mol cell*. 2005;18:601–7.
- Yan B, Liu Y, Bai H, Chen M, Xie S, Li D, et al. HDAC6 regulates IL-17 expression in T lymphocytes: implications for HDAC6-targeted therapies. *Theranostics* 2017;7:1002–9.
- de Zoeten EF, Wang L, Butler K, Beier UH, Akimova T, Sai H, et al. Histone deacetylase 6 and heat shock protein 90 control the functions of Foxp3(+) T-regulatory cells. *Mol Cell Biol*. 2011;31:2066–78.
- Laino AS, Betts BC, Veerapathran A, Dolgalev I, Sarnaik A, Quayle SN, et al. HDAC6 selective inhibition of melanoma patient T-cells augments anti-tumor characteristics. *J Immunother Cancer*. 2019;7:33.
- Fukumoto T, Fatkhutdinov N, Zundell JA, Tcyganov EN, Nacarelli T, Karakashev S, et al. HDAC6 Inhibition Synergizes with Anti-PD-L1 Therapy in ARID1A-Inactivated Ovarian Cancer. *Cancer Res*. 2019;79:5482–9.
- Pamer EG. Immune responses to *Listeria monocytogenes*. *Nat Rev Immunol*. 2004;4:812–23.
- Zhan Y, Cheers C. Control of IL-12 and IFN-gamma production in response to live or dead bacteria by TNF and other factors. *J Immunol (Baltim, Md: 1950)*. 1998;161:1447–53.
- Moreno-Gonzalo O, Ramirez-Huesca M, Blas-Rus N. HDAC6 controls innate immune and autophagy responses to TLR-mediated signalling by the intracellular bacteria *Listeria monocytogenes*. 2017; 13: e1006799.
- Zhang YS, Xin DE, Wang Z, Song X, Sun Y, Zou QC, et al. STAT4 activation by leukemia inhibitory factor confers a therapeutic effect on intestinal inflammation. *The EMBO journal*. 2019;38.
- Nguyen KB, Watford WT, Salomon R, Hofmann SR, Pien GC, Morinobu A, et al. Critical role for STAT4 activation by type 1 interferons in the interferon-gamma response to viral infection. *Science* 2002;297:2063–6.
- Nguyen HN, Noss EH, Mizoguchi F, Huppertz C, Wei KS, Watts GF, et al. Autocrine Loop Involving IL-6 Family Member LIF, LIF Receptor, and STAT4 Drives Sustained Fibroblast Production of Inflammatory Mediators. *Immunity* 2017;46:220–32.
- Wei L, Vahedi G, Sun H-W, Watford WT, Takatori H, Ramos HL, et al. Discrete roles of STAT4 and STAT6 transcription factors in tuning epigenetic modifications and transcription during T helper cell differentiation. *Immunity* 2010;32:840–51.
- Vahedi G, Takahashi H, Nakayama S, Sun H-W, Sartorelli V, Kanno Y, et al. STATs shape the active enhancer landscape of T cell populations. *Cell* 2012;151:981–93.
- Nakayama S, Kanno Y, Takahashi H, Jankovic D, Lu KT, Johnson TA, et al. Early Th1 cell differentiation is marked by a Tfh cell-like transition. *Immunity* 2011;35:919–31.
- Weinstein JS, Laidlaw BJ, Lu Y, Wang JK, Schulz VP, Li N, et al. STAT4 and T-bet control follicular helper T cell development in viral infections. *J Exp Med*. 2018;215:337–55.
- Wada H, Masuda K, Satoh R, Kakugawa K, Ikawa T, Katsura Y, et al. Adult T-cell progenitors retain myeloid potential. *Nature* 2008;452:768–72.
- Luc S, Luis TC, Boukarabila H, Macaulay IC, Buza-Vidas N, Bouriez-Jones T, et al. The earliest thymic T cell progenitors sustain B cell and myeloid lineage potential. *Nat Immunol*. 2012;13:412–9.
- Henry CJ, Ornelles DA, Mitchell LM, Brzoza-Lewis KL, Hiltbold EM. IL-12 produced by dendritic cells augments CD8 + T cell activation through the production of the chemokines CCL1 and CCL17. *J Immunol*. 2008;181:8576–84.

26. Vacaflares A, Freedman SN, Chapman NM, Houtman JC. Pretreatment of activated human CD8 T cells with IL-12 leads to enhanced TCR-induced signaling and cytokine production. *Mol Immunol*. 2017;81:1–15.
27. Wilson DC, Matthews S, Yap GS. IL-12 signaling drives CD8 + T cell IFN-gamma production and differentiation of KLRG1 + effector subpopulations during *Toxoplasma gondii* Infection. *J Immunol*. 2008;180:5935–45.
28. Ma L, Huang C, Wang XJ, Xin DE, Wang LS, Zou QC, et al. Lysyl Oxidase 3 Is a Dual-Specificity Enzyme Involved in STAT3 Deacetylation and Deacetylimination Modulation. *Mol cell*. 2017;65:296–309.
29. Skene PJ, Henikoff JG, Henikoff S. Targeted in situ genome-wide profiling with high efficiency for low cell numbers. *Nat Protoc*. 2018;13:1006–19.
30. Bergstrom KS, Morampudi V, Chan JM, Bhinder G, Lau J, Yang H, et al. Goblet Cell Derived RELM-beta Recruits CD4 + T Cells during Infectious Colitis to Promote Protective Intestinal Epithelial Cell Proliferation. *PLoS Pathog*. 2015;11:e1005108.

ACKNOWLEDGEMENTS

We are grateful to Yu Zhang for providing us with the *Hdac6*^{-/-} mice. Jingjing Wang and Qi Li for technical help in *L. monocytogenes* infection experiments. We are grateful to Bing Su for manuscript review and discussion.

AUTHOR CONTRIBUTIONS

YZ and DX contributed to the experimental design, conceptions of experiments, and manuscript preparation. ZW and WP performed the experiments, data analysis and manuscript preparation. YZ, JL, MX, NC, JZ, YJ, MC and YW assisted with the experiments. MC and JY provided technical assistance. ZC, XL and LC contributed to the data analysis and manuscript writing. YC was involved in the conception of the research, experimental design, data analysis, and manuscript preparation.

FUNDING

YZ was supported by the Young Scientists Fund of the National Natural Science Foundation Grant of China (32000620). This work was supported by National Natural Science Foundation Grant of China (81820108023, U1603284 and 81530083), Young Scientists Fund of the National Natural Science Foundation Grant of China (31700789), National Key Research and Development Program of China (2016YFC1302402), and the Priority Academic Program Development of Jiangsu Higher Education Institutions (PAPD).

COMPETING INTERESTS

The authors declare no competing interests.

ETHICS APPROVAL

All animal experiments were performed in compliance with the guide for the care and use of laboratory animals and were approved by the institutional biomedical research ethics committee of Soochow University.

ADDITIONAL INFORMATION

Supplementary information The online version contains supplementary material available at <https://doi.org/10.1038/s41418-022-01017-9>.

Correspondence and requests for materials should be addressed to Y. Eugene Chinn.

Reprints and permission information is available at <http://www.nature.com/reprints>

Publisher's note Springer Nature remains neutral with regard to jurisdictional claims in published maps and institutional affiliations.